








Protection of Ising spin-orbit coupling in bulk misfit superconductors

Tomas Samuely,^{1,*} Darshana Wickramaratne²,,² Martin Gmitra²,,^{1,3} Thomas Jaouen,⁴ Ondrej Šofranko,¹ Dominik Volavka¹,,¹ Marek Kuzmiak³,,³ Jozef Haniš¹,,¹ Pavol Szabó,³ Claude Monney,⁵ Geoffroy Kremer,^{5,6} Patrick Le Fèvre,⁷ François Bertran,⁷ Tristan Cren,⁸ Shunsuke Sasaki⁹,,⁹ Laurent Cario,⁹ Matteo Calandra,¹⁰ Igor I. Mazin,^{11,†} and Peter Samuely³

¹*Institute of Physics, Faculty of Science, Pavol Jozef Šafárik University in Košice, 04001 Košice, Slovakia*

²*Center for Computational Materials Science, U.S. Naval Research Laboratory, Washington, DC 20375, USA*

³*Centre of Low Temperature Physics, Institute of Experimental Physics, Slovak Academy of Sciences, 04001 Košice, Slovakia*

⁴*Univ Rennes, CNRS, (IPR Institut de Physique de Rennes) - UMR 6251, F-35000 Rennes, France*

⁵*Département de Physique and Fribourg Center for Nanomaterials, Université de Fribourg, Fribourg CH-1700, Switzerland*

⁶*Institut Jean Lamour, UMR 7198, CNRS-Université de Lorraine, Campus ARTEM, 2 allée André Guinier, BP 50840, 54011 Nancy, France*

⁷*SOLEIL synchrotron, L'Orme des Merisiers, Départementale 128, F-91190 Saint-Aubin, France*

⁸*Institut des NanoSciences de Paris, Sorbonne Université and CNRS-UMR 7588, Paris 75005, France*

⁹*Nantes Université, CNRS, Institut des Matériaux de Nantes Jean Rouxel, IMN, F-44000 Nantes, France*

¹⁰*Dipartimento di Fisica, Università di Trento, via Sommarive 14, I-38123 Povo, Italy*

¹¹*Department of Physics and Astronomy and Quantum Science and Engineering Center,*

George Mason University, Fairfax, Virginia 22030, USA



(Received 18 September 2023; accepted 13 November 2023; published 4 December 2023)

Ising superconductivity is present due to the combined effect of broken-inversion symmetry and spin-orbit coupling that locks the spins out of plane, features that are associated with two-dimensional materials. We show that bulk misfit superconductors, $(\text{LaSe})_{1.14}(\text{NbSe}_2)$ and $(\text{LaSe})_{1.14}(\text{NbSe}_2)_2$, comprising monolayers and bilayers of NbSe_2 , exhibit unexpectedly strong Ising protection with a Pauli-limit violation comparable to monolayer NbSe_2 . We establish these misfit compounds as Ising superconductors using complementary experimental methods in combination with first-principles calculations. A concerted effect of charge-transfer, defects, reduction of interlayer hopping, and stacking enables Ising superconductivity in these compounds and therefore provides a possible pathway to design of bulk superconductors that are resilient to magnetic fields.

DOI: [10.1103/PhysRevB.108.L220501](https://doi.org/10.1103/PhysRevB.108.L220501)

In superconductors, an external magnetic field can break the Cooper pairs via two mechanisms. The first is orbital pair breaking due to the Lorentz force exerted by this field. This does not occur in two-dimensional (2D) superconductors if the magnetic field is in plane. The second mechanism is spin-pair breaking due to Zeeman shifts of opposite signs on the antiparallel spins in a spin-singlet Cooper pair. The minimum field to break pairs is the Pauli paramagnetic limit B_P [1,2]. It can be understood from the energy balance: in the normal (but not in the superconducting) state, an external field B is Pauli screened, with an energy gain of $\chi_{\text{Pauli}} B^2/2$, where χ_{Pauli} is the Pauli susceptibility determined by the density of states, $N(E_F)$, at the Fermi level (E_F). In the BCS theory the pairing energy is $N(E_F) \Delta^2/2$, where Δ is the superconducting energy gap. Hence, when B_P exceeds Δ , it is energetically favorable to destroy superconductivity.

A superconducting state that can screen an external field is not subject to Pauli-limiting pair breaking, such as in some triplet superconductors [3]. Recently discovered Ising superconductors (IS) are also not Pauli limited for in-plane

magnetic fields. Their spin-orbit coupling (SOC) splits the bands and leads to electron spins that are perpendicular to the 2D plane with the spins of the SOC-partner states aligned antiparallel. One consequence is that the Pauli screening for in-plane magnetic fields is affected by the SOC split states that are removed from the Fermi level and therefore not affected by superconductivity [4]. As long as both the Zeeman shift and Δ are small compared to the SOC splitting (i.e., many hundreds of tesla in NbSe_2) the Pauli pair breaking is absent [5–12]. This is not unrelated to the resilience of triplet superconductivity to magnetic fields: in IS half of the Cooper pairs are described as singlet + triplet, and half as singlet–triplet [4]. The absence of inversion symmetry is a prerequisite for SOC to lift the Kramers degeneracy. In the canonical IS, NbSe_2 , this is satisfied in a monolayer, but not in a bilayer or bulk, preventing IS in bulk NbSe_2 [5]. In this study we report experiments and theory that clearly demonstrate that bulk layered compounds containing NbSe_2 can exhibit Ising protection [13,14]. Here, the broken-inversion symmetry is a necessary but insufficient ingredient, and we will show the energy scales of interlayer coupling with respect to spin-orbit coupling also matters to attain Ising protection.

Figures 1(a) and 1(b) illustrate the two compounds that we synthesize and investigate, $(\text{LaSe})_{1.14}(\text{NbSe}_2)$ and

*tomas.samuely@upjs.sk

†imazin2@gmu.edu

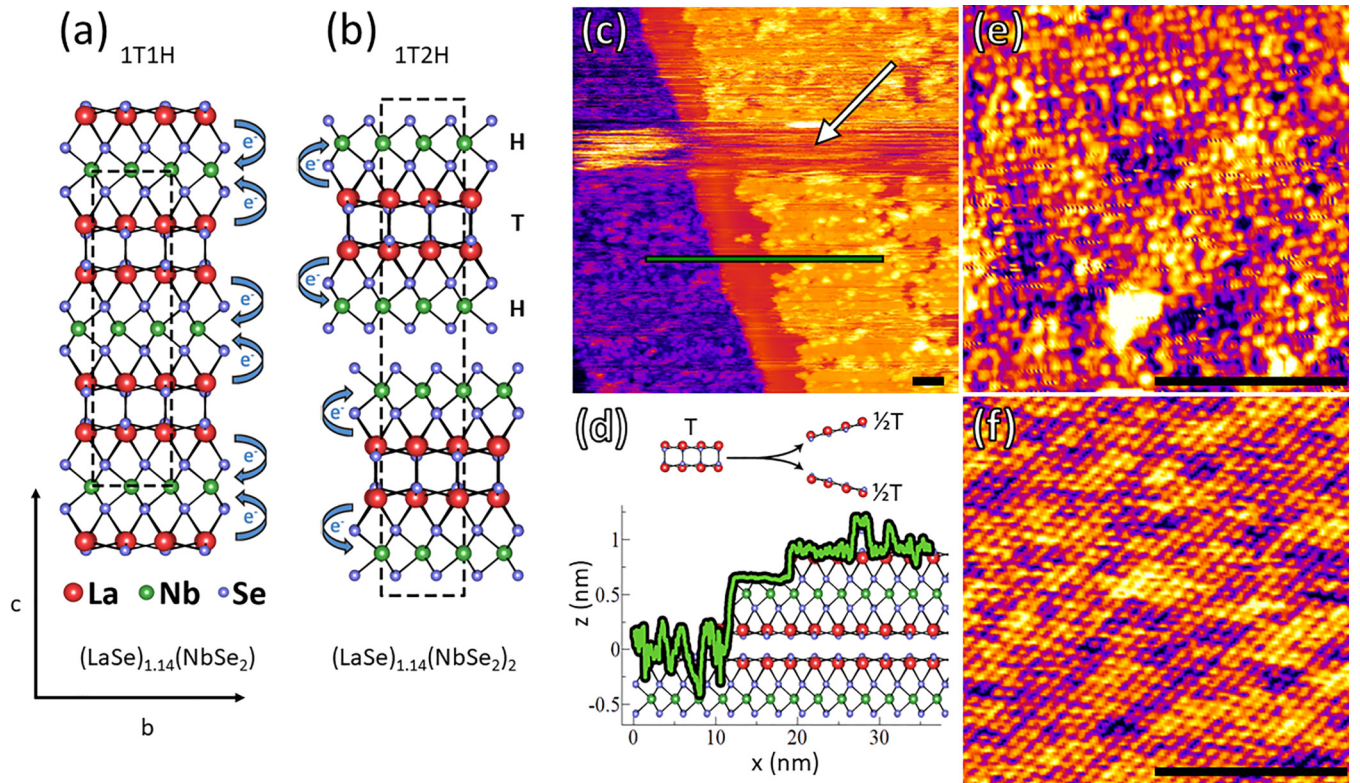


FIG. 1. Crystal structure of (a) 1T1H and (b) 1T2H. Dashed rectangles represent unit cell in bc plane. (c) Topography of three atomic terraces of 1T1H, H surface in middle and $\frac{1}{2}$ -T surfaces adjacent to H surface. White arrow indicates area where scanning tip disrupted unstable $\frac{1}{2}$ -T layer. (d) (Top) Schematic illustration of how T layer of 1T1H can be cleaved into two $\frac{1}{2}$ -T layers. (Bottom) Height profile along green line in (c), imposed on illustrated atomic structure of H and T layers. Vertical size of illustrated atomic structure is to scale while horizontal size is exaggerated for clarity. Height profile reveals step size between NbSe_2 , and $\frac{1}{2}$ -T layer terrace is 3 \AA , i.e., half size of full T layer. (e) Topography of cleaved $\frac{1}{2}$ -T layer of 1T1H revealing imperfect tetragonal lattice. Large white spot corresponds to residue of removed top $\frac{1}{2}$ -T surface and dark spots correspond to vacancy sites. (f) Topography of H layer of 1T1H with hexagonal lattice after removing unstable $\frac{1}{2}$ -T layer by continuously sweeping area with STM tip. Periodicity of imaged T and H lattices is also visible in fast Fourier transform of (e) and (f) along with more intricate details stemming from misfit properties, described in Supplemental Material [18]. Scalebars in (c), (e), and (f) represent 5 nm .

$(\text{LaSe})_{1.14}(\text{NbSe}_2)_2$. Since the 2D lattice of LaSe is tetragonal and that of NbSe_2 is hexagonal, we refer to the compounds as 1T1H and 1T2H, respectively. Previous work has shown that both are superconducting with $T_c = 1.23$ and 5.7 K , respectively, and they both exhibit an in-plane critical field $B_{c2//ab}$ that strongly exceeds the Pauli limit B_P [13]. For $(\text{LaSe})_{1.14}(\text{NbSe}_2)_2$ the ratio of $B_{c2//ab}/B_P$ is ~ 5 ; for $(\text{LaSe})_{1.14}(\text{NbSe}_2)$ it is ~ 10 —a clear signature of IS in bulk compounds. Their fundamental structural units are monolayers of NbSe_2 , where Nb atoms are in a trigonal prismatic coordination with Se, and LaSe with a rocksalt structure. A stoichiometric compound of NbSe_2 and LaSe forms when one of the constituent substructures distorts to accommodate the lattice parameters of the second substructure; hence, they are often referred to as misfit compounds [15]. One unit cell of NbSe_2 has a basal plane area of 10.25 \AA^2 [16], while 1 unit cell of LaSe has an area of 9.19 \AA^2 [17]; their ratio is larger than 1 and leads to the two misfit compounds we investigate.

In 1T2H, the H-T-H (NbSe_2 – LaSe – NbSe_2) trilayers are vertically stacked via van der Waals interactions [15], whereas 1T1H forms a fully three-dimensional ionocovalent crystal [18]. This is corroborated by our first-principles calculations of the cohesive energy. The calculated energy to split the

isolated T layer into two $\frac{1}{2}$ -T layers [Fig. 1(d)] is $E_T \approx -56.8 \text{ meV/\AA}^2$, which is lower than the cohesive energy $E_{T-H} \approx -100 \text{ meV/\AA}^2$ that binds the T and H layers. This prediction is consistent with our scanning tunneling microscopy (STM), illustrated in Figs. 1(c)–1(f), where the $\frac{1}{2}$ -T layer is seen to be much less stable than the H surface layer. Indeed, we were unable to image the $\frac{1}{2}$ -T layer unless the sample was cleaved at liquid nitrogen temperature and subsequently scanned *in situ* in ultrahigh vacuum.

Considering the oxidation numbers La^{3+} , Se^{2-} , and Nb^{3+} , the excess stoichiometry of the T layer (1.14) with respect to the H layer suggests a charge transfer of $0.57e^-$ per Nb, from the T layer into the two adjacent H layers in 1T2H. The estimated carrier density is then $n_{\text{est}} = 4.6 \times 10^{21} \text{ cm}^{-3}$, based on the NbSe_2 unit-cell lattice parameters [15]. The 1T2H Hall coefficient at 300 K is $R_H \approx +1.45 \pm 0.1 \times 10^{-9} \text{ m}^3/\text{C}$ [Fig. 2(a)], corresponding to a charge-carrier density $n \approx 4.7 \times 10^{21} \text{ cm}^{-3}$. The positive sign is consistent with transport occurring via the Nb $4d$ hole pocket and the measured carrier density agrees with our estimate above, and prior measurements [14].

For 1T1H, the same arguments suggest that each H layer accepts $1.14e^-$ per Nb from the two adjacent $\frac{1}{2}$ -T layers.

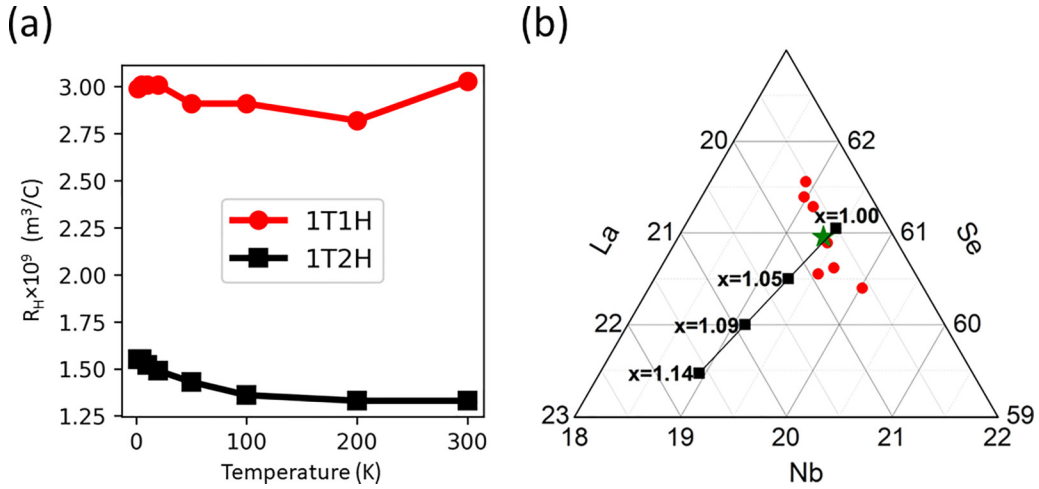


FIG. 2. (a) Hall coefficients of 1T1H (red dots) and 1T2H (black squares). (b) Projections of energy-dispersive x-ray spectroscopic analyses for $\text{La}_x\text{Se}_{1.14}\text{NbSe}_2$ crystals in La–Nb–Se ternary diagram (atomic percentages). Red dots are mean analyses of each crystal, while green star represents mean value for seven crystals. Black line represent theoretical compositions calculated between vacancy-rich ($x = 1$) and vacancy-free ($x = 1.14$) poles. Mean experimental composition lies on this line and evidences amount of La vacancies around 11.1%. More details in Supplemental Material [18].

However, based on the formal oxidation states, each Nb can accept a maximum of $1e^-$, leaving $0.14e^-$ per La within the T layer. First-principles calculations confirm these considerations and show the Nb $4d$ hole band at the K point is occupied (Supplemental Material, Fig. S3(a) [19]), while the partially filled La $5d$ electron band crosses the Fermi level at the Γ point (Supplemental Material, Fig. S3(b) [19]). Hall measurements indicate mobile holes with a Hall coefficient $R_H \approx +3 \times 10^{-9} \text{ m}^3/\text{C}$ [Fig. 2(a)], in contrast with the negative Hall coefficient expected if transport occurs via the LaSe conduction band. The carrier density at 300 K from the Hall coefficient is $n \approx 2 \times 10^{21} \text{ cm}^{-3}$, or $0.75e^-$ per Nb atom. Though this doping is larger than in the 1T2H structure, it is well below the maximum possible doping of $1e^-$ per Nb.

While evidence of La with a formal valence lower than 3 has been found in other layered compounds [20], a more plausible explanation of this discrepancy is deviations from stoichiometry. Point defects that act as acceptors can compensate the charge transferred into NbSe_2 and lower the effective doping. We consider the role of La vacancies in LaSe, motivated by the fact that prior work on other misfit compounds identified cation vacancies [21–23]. Figure 2(b) summarizes our energy-dispersive x-ray spectroscopy (EDS) measurements of sample composition. Despite small variations over different crystals, the mean composition indicates a La vacancy concentration of 11.1%, suggesting that 0.76 electrons were transferred per Nb atom, in agreement with the Hall data.

Our angle-resolved photoemission spectroscopy (ARPES) measurements of 2H- NbSe_2 , 1T2H, and 1T1H [Figs. 3(a)–3(c)] show that the Nb $4d$ states crossing E_F shift towards higher binding energies, as expected with electron doping of the H layer. Furthermore, the Nb $4d$ hole band is not completely filled in the 1T1H structure, consistent with our positive Hall coefficient.

At the $\bar{K}(\bar{K}')$ points, E_F lies very close to the top of the Nb $4d$ band. In bulk 2H- NbSe_2 the Fermi surface around the

K points comprises two spin-degenerate trigonally warped barrels formed by the Nb $4d$ bands [27]. These bands, split by interlayer coupling, are visible around $k_x = \pm 0.8 \text{ \AA}^{-1}$ in the out-of-plane momentum (k_z) map. Figure 3(e) shows their weak, but finite, k_z dispersion as the outer Γ pocket around $k_x = \pm 0.5 \text{ \AA}^{-1}$. In contrast to the Nb $4d$ states whose wave functions are mainly localized within individual layers of the unit cell, the inner Γ pocket is derived from the Se $4p_z$ orbital that is delocalized over the two NbSe_2 layers of the unit cell and therefore strongly dispersed in k_z as seen at the zone center. The quasi-2D nature of the electronic structure of the 1T2H misfit compound is evident in Fig. 3(f). Only the outer Γ pocket remains, around a reduced k_x value of $\pm 0.4 \text{ \AA}^{-1}$, due to the electron doping, and no k_z dispersion is visible.

Using the Fermi wave vectors, k_F^{1T2H} and k_F^{1T1H} , of the misfit's $\bar{\Gamma}$ pockets in Figs. 3(g) and 3(h) we estimate the charge transfer in 1T1H by comparing the areas of the Fermi surface. We obtain a ratio of the hole densities $\frac{n_{2D}^{1T1H}}{n_{2D}^{1T2H}} = \left(\frac{k_F^{1T1H}}{k_F^{1T2H}}\right)^2 \approx 0.43$. Assuming that LaSe transfers $0.57e^-$ per Nb atom in 1T2H, the charge transfer obtained from ARPES in 1T1H is $0.82e^-$ per Nb atom, which compares well with the $0.75e^-$ obtained from the Hall and EDS measurements.

Figure 4 illustrates the calculated band structure of the monolayer NbSe_2 , stoichiometric 1T2H and off-stoichiometric 1T1H with a La vacancy concentration of 12.5% comparable to the experimentally estimated value of 11.1%. For the misfit compounds, a large amount of electron doping into the H layer shifts the E_F towards the top of the Nb $4d$ hole band at the K point, consistent with our ARPES and Hall measurements.

Microscopic mechanisms behind the Ising protection. To provide insight into how Ising protection arises in these compounds we start with the 1T1H structure. Consider a NbSe_2 bilayer, where the combination of inversion symmetry and SOC leads to a pair of doubly degenerate states at K and

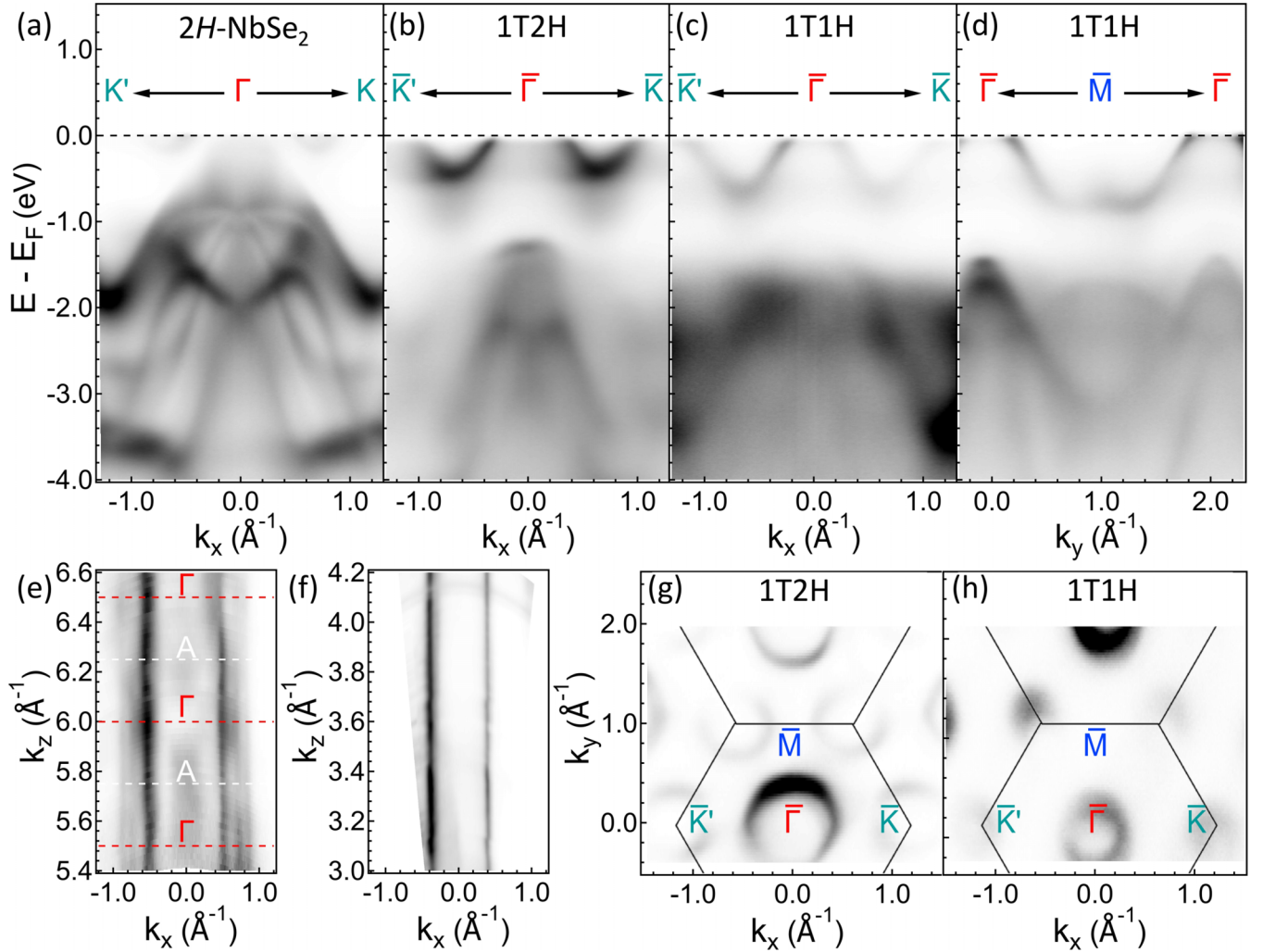


FIG. 3. (a) ARPES map along $K' - \Gamma - K$ high-symmetry line of hexagonal Brillouin zone of $2H\text{-NbSe}_2$. $h\nu = 106$ eV. (b) ARPES map along $\bar{K}' - \bar{\Gamma} - \bar{K}$ of $1T2H$ [$(\text{LaSe})_{1.14}(\text{NbSe}_2)_2$]. (c), (d) ARPES maps along $\bar{K}' - \bar{\Gamma} - \bar{K}$ and $\bar{\Gamma} - \bar{M} - \bar{\Gamma}$ of $1T1H$ [$(\text{LaSe})_{1.14}(\text{NbSe}_2)$]. $h\nu = 150$ eV for both misfits. (e), (f) Out-of-plane momentum (k_z) dispersions at $k_y = 0 \text{ \AA}^{-1}$ and E_F for NbSe_2 and $1T2H$. $h\nu = 100 - 160$ eV and $h\nu = 20 - 60$ eV for $2H\text{-NbSe}_2$ and $1T2H$, respectively. Inner potential of 17.6 eV [24] and work function value of 5.9 eV [25] were used for converting photon energies into k_z values within free-electron final-state approximation. Integer and half-integer values of k_z correspond to Γ points in $2H\text{-NbSe}_2$ (out-of-plane lattice parameter $c = 12.5 \text{ \AA}$) [26]. (g), (h) Fermi surfaces of $1T2H$ (g) and $1T1H$ (h) with overlaid hexagonal surface Brillouin zones of $2H\text{-NbSe}_2$ and associated $\bar{\Gamma}$, \bar{K} , \bar{K}' , and \bar{M} high-symmetry points.

K' , and an interlayer hopping, which we approximate as a constant, t . The magnitude of t in the $1T1H$ compound is different from that in the pristine NbSe_2 bilayer since the separation between the H layers increases by $\sim 5.6 \text{ \AA}$ and the interlayer tunneling proceeds through the T layer rather than vacuum. We can use a 4×4 Hamiltonian to represent the spin-up and -down states in each NbSe_2 layer and calculate the electronic structure. By accounting for SOC, effective interlayer hopping, and a Zeeman term due to an applied magnetic field, one can show the Pauli susceptibility has two principal contributions: one from electrons at E_F , and the other from the states split off by SOC that are farther away from E_F . The former term disappears in the superconducting state; the latter does not. The thermodynamic balance that determines the critical field is defined as $(\chi_n - \chi_s)B_t^2 = N(E_F)\Delta^2$ [28], where $\chi_n = \chi_{\text{Pauli}}$ is the susceptibility in the normal state, χ_s is the susceptibility in the superconducting state, and B_t

is the thermodynamic critical field. For a bilayer with SOC and an effective interlayer hopping t , we get $\chi_s = \chi_{\text{Pauli}} \frac{\zeta^2}{\zeta^2 + t^2}$. In $1T1H$ the spin-split bands at the K point are separated by ~ 150 meV [Fig. 4(c)]; therefore ζ , which is half of the spin-orbit splitting, is ~ 75 meV. Now, t is 1/4 of the bandwidth along the out-of-plane direction. The out-of-plane bandwidth is k dependent, the dispersion is flat along $K-H$, i.e., $t \sim 0$, while it is finite but small along $\Gamma-A$. We estimate the effective hopping relevant for the Ising protection as $t \sim 25$ meV. This leads to an enhancement of the critical field over B_P by a factor $B_P \frac{\sqrt{\zeta^2 + t^2}}{t} \sim 3B_P$. Therefore, the $1T1H$ crystal can be considered as an “infinite” stack of rigidly doped NbSe_2 monolayers with extremely weak interlayer hopping via LaSe layers. This Ising protection due to reduced interlayer hopping is also consistent with the conjecture by Xi *et al.* [5] regarding the Pauli violation for bilayer and trilayer NbSe_2 .

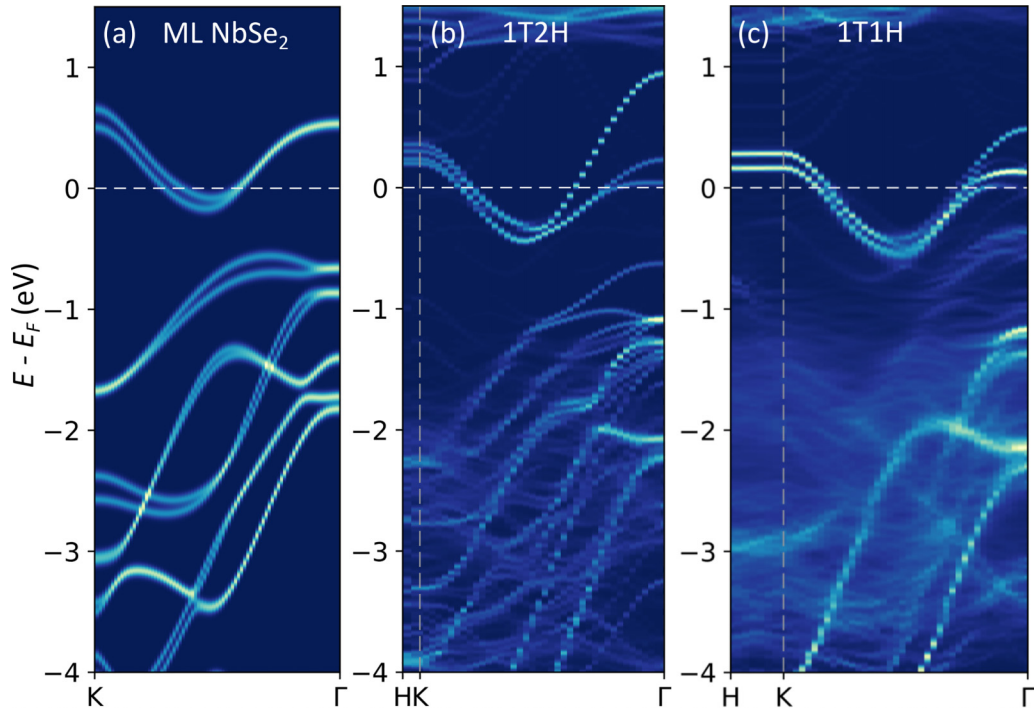


FIG. 4. Electronic structures unfolded onto hexagonal Brillouin zone along high-symmetry lines. (a) Band structure for supercell calculations of bare monolayer of NbSe₂ (b) 1T2H and (c) 1T1H with 12.5% La vacancies.

In 1T2H, the structure can be viewed as a stack of seemingly centrosymmetric 2H-NbSe₂ bilayers separated by LaSe misfit layers [Fig. 1(b)]. Here, we replace t with a much larger number t_0 to account for the stronger interlayer coupling within the bilayer structure. If one assumes that $t_0 \sim 2\zeta$, as it is in bulk NbSe₂, we find the critical field is enhanced by a factor of $1.12B_p$, lower than the factor of 5 observed in our experiments. To resolve this discrepancy, we account for the fact that the LaSe layers below and above the NbSe₂ bilayer are oriented differently with respect to NbSe₂, thus breaking the total inversion symmetry in the misfit [15]. We emulate this effect in our theory by applying a constant energy shift of $\pm T_0$ to the upper and lower layers of the bilayer, which lifts the Kramers degeneracy. In Fig. 4(b), two pairs of NbSe₂ bands are present at the K point. Each pair is spin split by ~ 110 meV and they are mutually shifted by ~ 50 meV at the K point [Fig. 4(b)].

This results in two effects: one, which is often considered in the discussion of single monolayers [29], leads to a canting of the spin directions away from the c axis. The resulting spin can be projected onto the out-of-plane direction, yielding an Ising component, and onto the ab plane, yielding planar components (Rashba and Dresselhaus). The latter has no Ising protection for in-plane magnetic fields [29], so it is often believed that breaking the intralayer mirror symmetry is detrimental for IS.

What has been missed previously is the second effect, which helps restore the Ising protection. If we solve our 4×4 Hamiltonian including the effect of T_0 , one can show that the Ising protection is now determined by the

larger of the two expressions; either $B_t = B_p \frac{\sqrt{\zeta^2 + t_0^2}}{t_0}$ or $\mu_B B_t = \sqrt{t_0^2 + (T_0 + \zeta)^2} - \sqrt{t_0^2 + (T_0 - \zeta)^2}$ [30]. In our case, $T_0 \sim 25$ meV at the K valley, which is half of the mutual shift of the spin-split bands. However, since it is k dependent, we consider $T_0 \sim 10$ meV as a lower bound. This, combined with $\zeta \sim 55$ meV and $t_0 = 2\zeta$, yields $B_t \sim 150$ T, demonstrating that a finite energy shift due to asymmetric encapsulation provides strong Ising protection. This Ising protection is likely to be further reduced due to an admixture of planar SOC [29] as we discuss above, but it is unlikely to overcome the large value of B_t .

Hence, this hierarchy of energy scales of interlayer coupling, namely, breaking of inversion symmetry by the LaSe layer, SOC, and the magnitude of the superconducting gap in the 1T1H and 1T2H compounds, provides a consistent picture for the strong Ising protection observed in these bulk compounds. This is different from the IS in the monolayer where only the last two energy scales are present. *A priori* it is not obvious that these bulk compounds exhibit a 2D-like electronic structure and Ising protection, which highlights the crucial role played by the experiments in combination with calculations reported here. Moreover, the presence of charge doping in these misfit compounds, larger than what can be achieved with traditional substitutional doping, introduces the possibility of shifting the Fermi level to be in between the two spin-split bands, which is predicted to give rise to topological superconductivity [4,31,32]. It is plausible that these insights can be extended to other misfit compounds and bulk structures comprising transition-metal

dichalcogenide layers, where large in-plane critical magnetic fields that exceed the Pauli limit have been reported but not identified as evidence of Ising superconductivity. This includes works on $(\text{SnSe})_{1.16}(\text{NbSe}_2)_2$ [33], $\text{Ba}_6\text{Nb}_{11}\text{S}_{28}$ [34], cation-intercalated NbSe_2 [35], and organometallic intercalated compounds of 2H-TaS_2 [36,37]. Future experiments and theory work to determine the electronic and structural properties for this broad range of potential bulk Ising superconductors will be of great interest.

We thank V. Tkáč and J. Cordiez for assistance with the Hall measurements and chemical analysis, respectively. This work was supported by Projects No. APVV-20-0425, No. APVV-SK-FR-22-0006, No. VEGA 2/0058/20 and COST Action No. CA21144 (SUPERQUMAP). The research lead-

ing to these results has received funding from the European Union's Horizon 2020 Research and Innovation Programme under Grant Agreement No. 824109 (European Microkelvin Platform). D.W. was supported by the Office of Naval Research (ONR) through the Naval Research Laboratory's Basic Research Program. I.I.M. was supported by ONR through Grant No. N00014-20-1-2345. C.M. and G.K. acknowledge financial support from the Swiss National Science Foundation (SNSF) Grant No. P00P2_170597. M.G. and J.H. acknowledge support by Projects No. APVV-SK-CZ-RD-21-0114, No. VEGA 1/0105/20, Slovak Academy of Sciences Project No. IMPULZ IM-2021-42, and Project No. FLAG ERA JTC 2021 2DSOTECH. S.S., L.C., and T.C. acknowledge financial support from the Agence Nationale de la Recherche ANR-21-CE30-0054-02.

-
- [1] B. S. Chandrasekhar, A note on the maximum critical field of high-field superconductors, *Appl. Phys. Lett.* **1**, 7 (1962).
- [2] A. M. Clogston, Upper limit for the critical field in hard superconductors, *Phys. Rev. Lett.* **9**, 266 (1962).
- [3] D. Aoki, K. Ishida, and J. Flouquet, Review of U-based ferromagnetic superconductors: Comparison between UGe_2 , URhGe , and UCoGe , *J. Phys. Soc. Jpn.* **88**, 022001 (2019).
- [4] D. Wickramaratne, S. Khmelevskiy, D. F. Agterberg, and I. I. Mazin, Ising superconductivity and magnetism in NbSe_2 , *Phys. Rev. X* **10**, 041003 (2020).
- [5] X. Xi, Z. Wang, W. Zhao, J. H. Park, K. T. Law, H. Berger, L. Forró, J. Shan, and K. F. Mak, Ising pairing in superconducting NbSe_2 atomic layers, *Nat. Phys.* **12**, 139 (2016).
- [6] J. M. Lu, O. Zheliuk, I. Leermakers, N. F. Q. Yuan, U. Zeitler, K. T. Law, and J. T. Ye, Evidence for two-dimensional Ising superconductivity in gated MoS_2 , *Science* **350**, 1353 (2015).
- [7] Y. Saito, Y. Nakamura, M. S. Bahramy, Y. Kohama, J. Ye, Y. Kasahara, Y. Nakagawa, M. Onga, M. Tokunaga, T. Nojima *et al.*, Superconductivity protected by spin-valley locking in ion-gated MoS_2 , *Nat. Phys.* **12**, 144 (2016).
- [8] W. Chen, Q. Zhu, Y. Zhou, and J. An, Topological Ising pairing states in monolayer and trilayer TaS_2 , *Phys. Rev. B* **100**, 054503 (2019).
- [9] P. Baidya, D. Sahani, H. K. Kundu, S. Kaur, P. Tiwari, V. Bagwe, J. Jesudasan, A. Narayan, P. Raychaudhuri, and A. Bid, Transition from three- to two-dimensional Ising superconductivity in few-layer NbSe_2 by proximity effect from van der Waals heterostacking, *Phys. Rev. B* **104**, 174510 (2021).
- [10] S. C. De La Barrera, M. R. Sinko, D. P. Gopalan, N. Sivadas, K. L. Seyler, K. Watanabe, T. Taniguchi, A. W. Tsen, X. Xu, D. Xiao *et al.*, Tuning Ising superconductivity with layer and spin-orbit coupling in two-dimensional transition-metal dichalcogenides, *Nat. Commun.* **9**, 1427 (2018).
- [11] E. Sohn, X. Xi, W. Y. He, S. Jiang, Z. Wang, K. Kang, J. H. Park, H. Berger, L. Forró, K. T. Law *et al.*, An unusual continuous paramagnetic-limited superconducting phase transition in 2D NbSe_2 , *Nat. Mater.* **17**, 504 (2018).
- [12] J. Cui, P. Li, J. Zhou, W.-Y. He, X. Huang, J. Yi, J. Fan, Z. Ji, X. Jing, F. Qu *et al.*, Transport evidence of asymmetric spin-orbit coupling in few-layer superconducting 1T^d - MoTe_2 , *Nat. Commun.* **10**, 2044 (2019).
- [13] P. Samuely, P. Szabó, J. Kačmarčík, A. Meerschaut, L. Cario, A. G. M. Jansen, T. Cren, M. Kuzmiak, O. Šofranko, and T. Samuely, Extreme in-plane upper critical magnetic fields of heavily doped quasi-two-dimensional transition metal dichalcogenides, *Phys. Rev. B* **104**, 224507 (2021).
- [14] R. T. Leriche, A. Palacio-Morales, M. Campetella, C. Tresca, S. Sasaki, C. Brun, F. Debontridder, P. David, I. Arfaoui, O. Šofranko *et al.*, Misfit layer compounds: A platform for heavily doped 2D transition metal dichalcogenides, *Adv. Funct. Mater.* **31**, 2007706 (2020).
- [15] R. Roesky, A. Meerschaut, J. Rouxel, and J. Chen, Structure and electronic transport properties of the misfit layer compound $(\text{LaSe})_{1.14}(\text{NbSe}_2)_2$, “ LaNb_2Se_5 ”, *Z. Anorg. Allg. Chem.* **619**, 117 (1993).
- [16] O. S. Rajora and A. E. Curzon, The preparation and X-ray diffraction study of the layer materials $\text{NbS}_x\text{Se}_{2-x}$ for $0 \leq x \leq 2$, *Phys. Status Solidi* **99**, 65 (1987).
- [17] P. Haen, H. Bioud, F. Lapierre, and F. Holtzberg, Kondo-type resistivity of mixed-valent Tm diluted in LaSe , *J. Magn. Magn. Mater.* **63**, 603 (1987).
- [18] A. Nader, A. Lafond, A. Briggs, A. Meerschaut, and R. Roesky, Structural characterization and superconductivity in the misfit layer compound $(\text{LaSe})_{1.14}(\text{NbSe}_2)$, *Synth. Met.* **97**, 147 (1998).
- [19] See Supplemental Material at <http://link.aps.org/supplemental/10.1103/PhysRevB.108.L220501> for details on sample preparation, experimental methods, first-principles calculations, estimation of La vacancies by EDS, STM topography, and calculated electronic structure of stoichiometric $1\text{T}^d\text{H}$, which includes Refs. [38–41].
- [20] I. I. Mazin, M. Shimizu, N. Takemori, and H. O. Jeschke, Novel Fe-based superconductor LaFe_2As_2 in comparison with traditional pnictides, *Phys. Rev. Lett.* **123**, 267001 (2019).
- [21] L. Cario, D. Johrendt, A. Lafond, C. Felser, A. Meerschaut, and J. Rouxel, Stability and charge transfer in the misfit compound $(\text{LaS})(\text{SrS})_{0.2}\text{CrS}_2$: *Ab initio* band-structure calculations, *Phys. Rev. B* **55**, 9409 (1997).
- [22] J. Rouxel, Y. Moëlo, A. Lafond, F. J. DiSalvo, A. Meerschaut, and R. Roesky, Role of vacancies in misfit layered compounds: The case of the gadolinium chromium sulfide compound, *Inorg. Chem.* **33**, 3358 (1994).

- [23] A. Meerschaut, Y. Moëlo, L. Cario, A. Lafond, and C. Deudon, Charge transfer in misfit layer chalcogenides, $[(MX)_n]_{1+x}(TX_2)_m$: A key for understanding their stability and properties, *Mol. Cryst. Liq. Cryst. Sci. Technol. Sect. A* **341**, 1 (2000).
- [24] K. Rossnagel, O. Seifarth, L. Kipp, M. Skibowski, D. Voß, P. Krüger, A. Mazur, and J. Pollmann, Fermi surface of $2H - NbSe_2$ and its implications on the charge-density-wave mechanism, *Phys. Rev. B* **64**, 235119 (2001).
- [25] T. Shimada and F. S. Ohuchi, Work function and photothreshold of layered metal dichalcogenides, *Jpn. J. Appl. Phys.* **33**, 2696 (1994).
- [26] F. Weber, R. Hott, R. Heid, L. L. Lev, M. Caputo, T. Schmitt, and V. N. Strocov, Three-dimensional Fermi surface of $2H-NbSe_2$: Implications for the mechanism of charge density waves, *Phys. Rev. B* **97**, 235122 (2018).
- [27] L. Bawden, S. P. Cooil, F. Mazzola, J. M. Riley, L. J. Collins-McIntyre, V. Sunko, K. W. B. Hunvik, M. Leandersson, C. M. Polley, T. Balasubramanian *et al.*, Spin-valley locking in the normal state of a transition-metal dichalcogenide superconductor, *Nat. Commun.* **7**, 11711 (2016).
- [28] K. Machida, Theory of magnetically polarizable superconductors, *J. Low. Temp. Phys.* **53**, 405 (1983).
- [29] D. Shaffer, J. Kang, F. J. Burnell, and R. M. Fernandes, Crystalline nodal topological superconductivity and Bogolyubov Fermi surfaces in monolayer $NbSe_2$, *Phys. Rev. B* **101**, 224503 (2020).
- [30] D. Wickramaratne, D. F. Agterberg, and I. I. Mazin (unpublished).
- [31] Y.-T. Hsu, A. Vaezi, M. H. Fischer, and E.-A. Kim, Topological superconductivity in monolayer transition metal dichalcogenides, *Nat. Commun.* **8**, 14985 (2017).
- [32] B. T. Zhou, N. F. Q. Yuan, H. L. Jiang, and K. T. Law, Ising superconductivity and Majorana fermions in transition-metal dichalcogenides, *Phys. Rev. B* **93**, 180501(R) (2016).
- [33] H. Bai, L. Qiao, M. Li, J. Ma, X. Yang, Y. Li, Q. Tao, and Z.-A. Xu, Multi-band superconductivity in a misfit layered compound $(SnSe)_{1.16}(NbSe_2)_2$, *Mater. Res. Express* **7**, 016002 (2020).
- [34] A. Devarakonda, H. Inoue, S. Fang, C. Ozsoy-Keskinbora, T. Suzuki, M. Kriener, L. Fu, E. Kaxiras, D. C. Bell, and J. G. Checkelsky, Clean 2D superconductivity in a bulk van der Waals superlattice, *Science* **370**, 231 (2020).
- [35] H. Zhang, A. Rousuli, K. Zhang, L. Luo, C. Guo, X. Cong, Z. Lin, C. Bao, H. Zhang, S. Xu *et al.*, Tailored Ising superconductivity in intercalated bulk $NbSe_2$, *Nat. Phys.* **18**, 1425 (2022).
- [36] R. A. Klemm, Pristine and intercalated transition metal dichalcogenide superconductors, *Physica C (Amsterdam, Neth.)* **514**, 86 (2015).
- [37] Y. Kashihara, A. Nishida, and H. Yoshioka, Upper and lower critical fields of TaS_2 (Pyridine) $_{1/2}$, *J. Phys. Soc. Jpn.* **46**, 1112 (1979).
- [38] G. Kresse and D. Joubert, From ultrasoft pseudopotentials to the projector augmented-wave method, *Phys. Rev. B* **59**, 1758 (1999).
- [39] J. P. Perdew, K. Burke, and M. Ernzerhof, Generalized gradient approximation made simple, *Phys. Rev. Lett.* **77**, 3865 (1996).
- [40] S. Grimme, J. Antony, S. Ehrlich, and H. Krieg, A consistent and accurate *ab initio* parametrization of density functional dispersion correction (DFT-D) for the 94 elements H-Pu, *J. Chem. Phys.* **132**, 154104 (2010).
- [41] V. Wang, N. Xu, J.-C. Liu, G. Tang, and W.-T. Geng, VASPKIT: A user-friendly interface facilitating high-throughput computing and analysis using VASP code, *Comput. Phys. Commun.* **267**, 108033 (2021).

Protection of Ising Spin-Orbit Coupling in Bulk Misfit Superconductors

Tomas Samuely^{1,*}, Darshana Wickramaratne², Martin Gmitra^{1,3}, Thomas Jaouen⁴, Ondrej Šofranko¹, Dominik Volavka¹, Marek Kuzmiak³, Jozef Haniš¹, Pavol Szabó³, Claude Monney⁵, Geoffroy Kremer^{5,6}, Patrick Le Fèvre⁷, François Bertran⁷, Tristan Cren⁸, Shunsuke Sasaki⁹, Laurent Cario⁹, Matteo Calandra¹⁰, Igor I. Mazin^{11,*}, Peter Samuely³

¹Institute of Physics, Faculty of Science, Pavol Jozef Šafárik University in Košice, 04001 Košice, Slovakia

²Center for Computational Materials Science, U.S. Naval Research Laboratory, Washington, DC 20375, USA

³Centre of Low Temperature Physics, Institute of Experimental Physics, Slovak Academy of Sciences, 04001 Košice, Slovakia

⁴Univ Rennes, CNRS, (IPR Institut de Physique de Rennes) - UMR 6251, F-35000 Rennes, France

⁵Département de Physique and Fribourg Center for Nanomaterials, Université de Fribourg, Fribourg CH-1700, Switzerland

⁶Institut Jean Lamour, UMR 7198, CNRS-Université de Lorraine, Campus ARTEM, 2 allée André Guinier, BP 50840, 54011 Nancy, France

⁷SOLEIL synchrotron, L'Orme des Merisiers, Départementale 128, F-91190 Saint-Aubin, France

⁸Institut des NanoSciences de Paris, Sorbonne Université and CNRS-UMR 7588, Paris 75005, France

⁹Institut des Matériaux Jean Rouxel, Université de Nantes and CNRS-UMR 6502, Nantes 44322, France

¹⁰Dipartimento di Fisica, Università di Trento, via Sommarive 14, I-38123 Povo, Italy

¹¹Department of Physics and Astronomy and Quantum Science and Engineering Center, George Mason University, Fairfax, VA 22030, USA

Supplemental material

Sample preparation

Single crystals of $(\text{LaSe})_{1.14}(\text{NbSe}_2)$ and $(\text{LaSe})_{1.14}(\text{NbSe}_2)_2$ were grown by chemical vapor transport using iodine and the product of the solid-state reaction of the elemental precursors (i.e., La, Nb, Se). More details of the 1T2H sample preparation are described in ref. [14]. 1T1H was prepared identically except for the molar ratio which was changed to $\text{La/Nb/Se} = 1.14/1/3.14$.

Energy-dispersive X-ray spectroscopy (EDS)

The chemical composition of 1T1H samples was inspected by energy-dispersive X-ray spectroscopy on a JEOL 5800LV scanning electron microscope equipped with a PGT microanalyzer and operating at 20 keV. Large crystals were pasted and mechanically pressed into carbon tape to reach a good horizontal alignment and improve accuracy.

Scanning tunnelling microscopy (STM)

Scanning tunnelling microscopy data was acquired in ultra-high vacuum at a base pressure lower than 10^{-10} mbar and a base temperature of 1.14 K using a mechanically cut gold tip operated in

the constant-current mode. Bias voltage of 1 V was applied to the sample, setpoint was 50 pA. The sample was mechanically cleaved in-situ at 77 K.

Hall measurements

The magnetotransport measurements were realized in a Quantum Design Physical Properties Measurement System using AC transport and resistivity options in the temperature range from 1.8 K to 300 K. Magnetic fields up to 9 T were applied in various orientations.

Angle-resolved photoemission spectroscopy (ARPES)

ARPES experiments were carried out at the CASSIOPEE beamline of the SOLEIL synchrotron radiation centre, in Saint-Aubin, France. The electron detector was a Scienta R4000 hemispherical analyser with an angular acceptance of $\pm 15^\circ$. The experiments were performed at $T = 14$ K with a linear horizontal (LH) polarization of the incident light. The total energy resolutions were between 30 meV and 80 meV depending on the measurements.

First-principles calculations

The electronic structure was calculated by means of density functional theory as implemented in the Vienna ab-initio simulation package VASP.6.2 [38]. The PAW pseudopotentials [38] were used with PBE exchange-correlation functional [39]. The lattice parameters and atomic positions within the structural models were relaxed with the force threshold below 2×10^{-2} eV \AA^{-1} . Dispersive van der Waals energy correction [40] was used for the 1T2H systems. The band structure unfolding was performed using VASPKIT [41]. The cleavage energy calculations were obtained from total energy calculations for a series of finite-size slabs with particular surface terminations.

Table SI. Chemical composition of the 1T1H samples determined by EDS.

Crystal (<i>n</i>)	Atomic composition (%)			Chemical formula		
	Se	Nb	La	Se	Nb	La
Crystal 1 (5)	61,29(12)	19,11(7)	19,60(7)	3,140(-)	0,979(6)	1,004(6)
Crystal 2 (5)	60,6(2)	19,52(14)	19,92(10)	3,140(-)	1,012(10)	1,033(8)
Crystal 3 (7)	61,56(5)	18,90(6)	19,54(7)	3,140(-)	0,964(4)	0,997(4)
Crystal 4 (5)	61,39(12)	18,97(13)	19,64(4)	3,140(-)	0,970(9)	1,005(4)
Crystal 5 (7)	60,62(13)	19,64(9)	19,74(6)	3,140(-)	1,017(7)	1,022(5)
Crystal 6 (8)	60,89(13)	19,44(9)	19,67(10)	3,140(-)	1,002(7)	1,014(7)
Crystal 7 (5)	60,4(2)	20,0(2)	19,58(7)	3,140(-)	1,041(12)	1,018(7)
Average	60,96(13)	19,37(10)	19,67(7)	3,140(-)	0,998(7)	1,013(6)
11,1% of La vacancies	60,93	19,40	19,67	3,140	1	1,014

Atomic percentages with relevant errors in brackets obtained by EDS analysis for seven different crystals of 1T1H (*n* is the number of measurements on each single crystal). To calculate the chemical formula, the amount of Selenium was fixed to 3.14 according to the theoretical chemical composition (LaSe)_{1.14}(NbSe₂). The last row represents the theoretical values of the atomic percentage and chemical formula for the case of a crystal with 11.1% La vacancies.

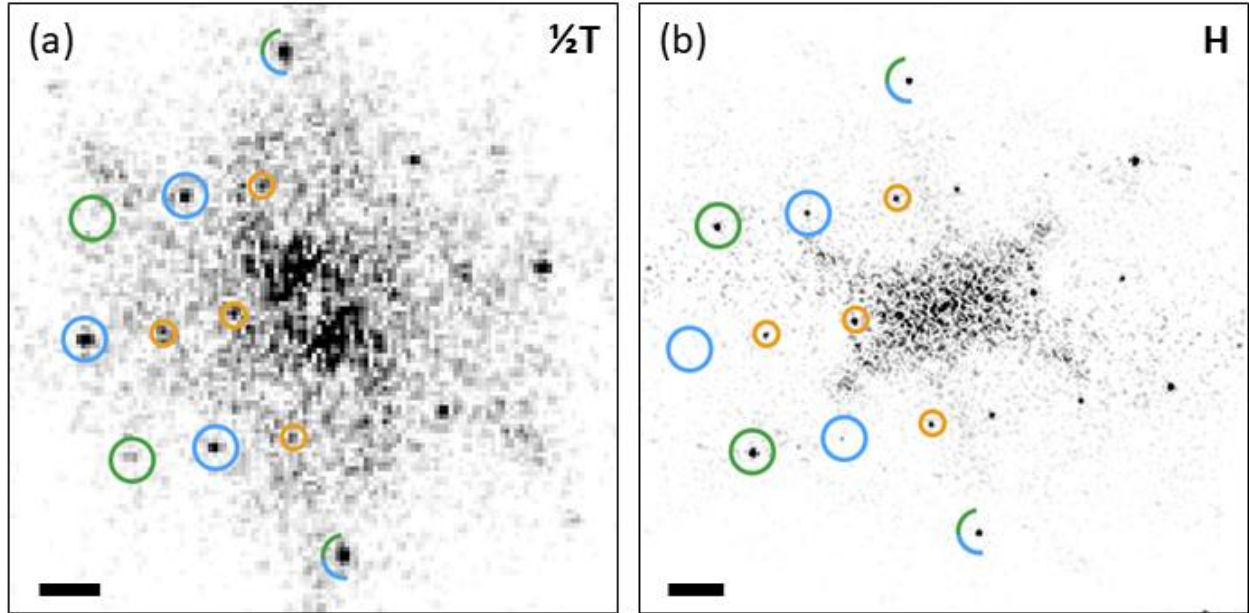


FIG. S1. (a) and (b) show the Fourier transform modulus of the topography in Figs. 1(e) and 1(f), respectively. In both FFT images both hexagonal and square Bragg peaks are present, denoted by green and blue circles, respectively, as well as peaks corresponding to the lattice modulations due to misfit, marked by orange circles. The blue-green semicircles belong simultaneously to the square and hexagonal lattice and lie in the commensurate b direction. The fact that both square and hexagonal lattices are present in both FFT images demonstrates the surface lattice modulation induced by the underlying layer. The scalebar represents 5 nm^{-1} .

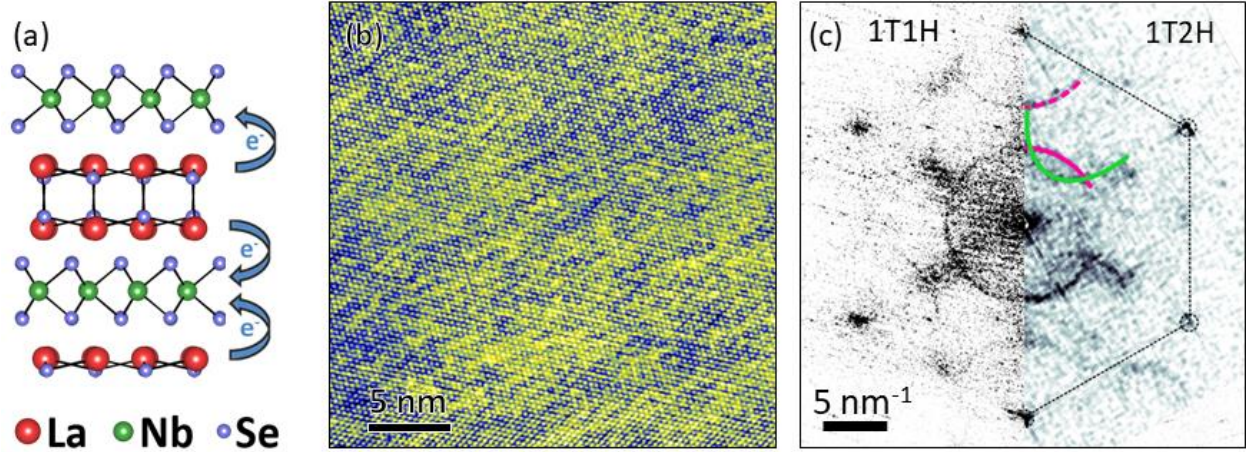


FIG. S2. (a) Crystal structure of 1T1H without the topmost $\frac{1}{2}$ T layer. (b) STM topography of the H layer of 1T1H after the unstable $\frac{1}{2}$ T layer was removed by continuously sweeping the area with STM tip (30nm x 30nm, $U_{bias} = 0.5$ mV, $I_{set} = 80$ pA, $T = 77$ K). (c) left: Fourier transform modulus of (b); right: Fourier transform modulus of 1T2H topography from ref. [14]. When the topmost $\frac{1}{2}$ T layer of 1T1H is removed, the H surface is charge-doped only by the underlying $\frac{1}{2}$ T layer, thus mimicking the situation in 1T2H as demonstrated in (a). Because the topography in (b) was acquired at low bias, i.e., energy close to E_F , it is possible to resolve the quasiparticle interference patterns in its Fourier transform. The fact that this pattern is almost identical to the 1T2H case, as demonstrated in (c), is well in line with the notion of the half-doped H surface layer. Though this is only a local surface effect not affecting the bulk properties of the crystal, it validates our qualitative understanding of the charge transfer between layers.

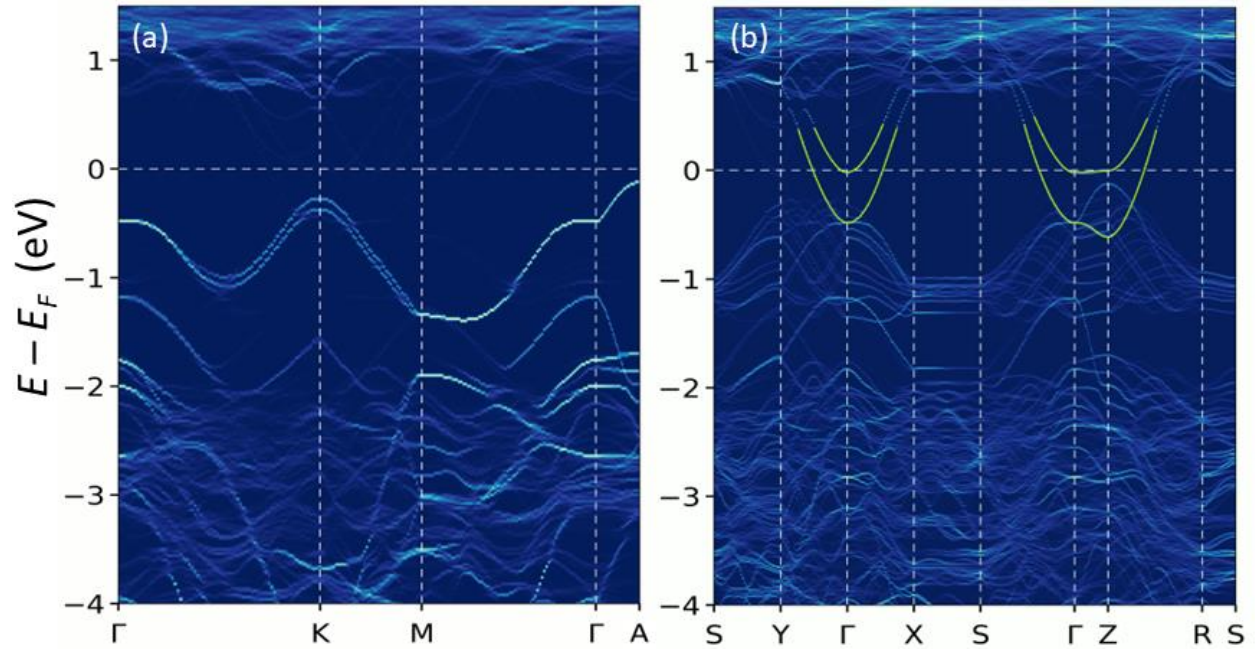


FIG. S3. Electronic band structure along high symmetry lines for stoichiometric bulk 1T1H calculated from first principles. Band structures are unfolded to (a) hexagonal and (b) orthorhombic Brillouin zones corresponding to zones for NbSe₂ and LaSe crystals. The partially filled La electron bands crossing the Fermi level at the Γ -point are highlighted in green.